REVIEW

PACS numbers: 25.20.-x; 52.50.Jm; 52.38.Kd
DOI: 10.1070/QE2001v031n11ABEH002081

Nuclear processes in a high-temperature plasma produced by an ultrashort laser pulse

A V Andreev, V M Gordienko, A B Savel'ev

Contents

***Abstract*. The experimental data on the initiation of a number of nuclear processes in a plasma produced by an ultrashort laser pulse of intensity $10^{16} - 10^{21}$ W cm^{-2} are summarised. These processes include excitation of nuclear levels, fusion and fission reactions, production of unstable isotopes, generation of ultrashort pulses of elementary particles, etc. The trends and outlook for studies aimed at increasing the intensity, energy, and average power of ultrashort laser pulses are analysed.**

Keywords: *superstrong light fields, plasma produced by an ultrashort laser pulse, nuclear processes.*

1. Introduction

In the last decade a great progress has been achieved in the development of a new generation of femtosecond solid-state lasers and laser systems. Femtosecond laser systems producing ultrashort light pulses (10 – 1000 fs) provide the peak pulse power up to 1 PW, while the peak intensity of focused laser beam achieves $10^{16} - 10^{21}$ W cm^{-2}. The problems of the development of such systems operating in different spectral ranges have been considered in papers [1 – 3]. Such systems can produce superstrong light fields under laboratory conditions, which cannot be obtained by other methods. Recall that for the laser radiation intensity up to $I \geqslant 10^{16}$ W cm^{-2}, the light field strength exceeds that of the intraatomic field in a hydrogen atom $E_a > 10^9$ V cm^{-1}. The use of superstrong light fields makes it possible to study the fundamental properties of matter in extreme and strongly nonequilibrium states and to perform nuclear physical experiments involving corpuscular and electromagnetic radiation produced by ultrashort laser pulses in a laser plasma (USP plasma).

The appearance of this new tool for studies has a revolutionary significance for physics, which can be compared to the creation of pulsed energy sources based on nuclear reactions. However, the fundamental difference is that a huge amount of energy $\sim 10^{11}$ J cm^{-3} is concentrated within a 'microvolume' as small as $\sim 10^{-11}$ cm^3. In addition, the cost of an experimental setup is drastically decreased. For the volume energy density of 10^{11} J cm^{-3}, the energy imparted to an atom is of the order of 10 MeV. Note for comparison that the energy required for the nuclear disintegration into individual nucleons is approximately equal to a product of the specific binding energy ε_b by the number A of nucleons, ε_b being equal to ~ 8 MeV for most nuclei, while the nuclear disintegration energy lies in the range from 2 to 20 MeV [4].

The action of laser radiation on a target is most efficient when the perturbation of a nuclear state is produced for the time during which the target material remains in a solid state. In this case, the concentration of laser photons with the energy ~ 1 eV should achieve $10^{28} - 10^{29}$ photon cm^{-3} for the rate of their incidence exceeding 10^{40} photon s^{-1} cm^{-3}.

Note that in a complete fission reaction of 1 kg of ^{235}U ($\rho = 19.5$ g cm^{-3}), the energy $\sim 10^{12}$ J cm^{-3} is released and the temperature achieves 10^8 K. The radiation intensity of a blackbody at a temperature of 10^8 K is $\sim 5 \times 10^{20}$ W cm^{-2}. Such radiation intensity can be achieved in modern petawatt

A V Andreev, V M Gordienko, A B Savel'ev Department of Physics, M V Lomonosov Moscow State University, Vorob'evy gory, 119899 Moscow, Russia

Received 5 April 2001
Kvantovaya Elektronika **31** (3) 941 – 956 (2001)
Translated by M N Sapozhnikov

laser systems [3], which can provide the energy density $\sim 10^{12}$ J cm^{-3} concentrated in a thin plasma layer [5].

Excitation by subpicosecond laser pulses with subpetawatt peak power is sufficient for the acceleration of plasma electrons to the energies required for the initiation of a variety of nuclear processes such as the excitation of nuclear levels, fusion and fission reactions, generation of elementary particles by ultrashort pulses, etc. (see Fig. 1).

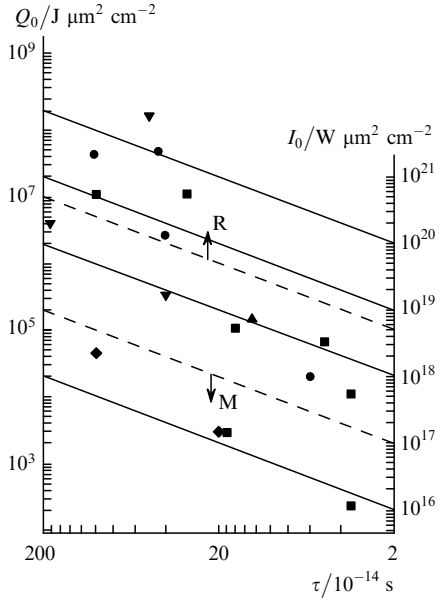

Figure 1. Nuclear processes in the USP plasma (experimental data from papers cited in the review): fusion reaction (■), photoexcitation of low-lying nuclear levels (◆), acceleration of protons (▼), generation of positrons (▲), photonuclear reactions (●). The dashed straight lines determine the boundary of the interaction in the regime of moderate (M) and relativistic (R) intensities; Q_0 and I_0 are the energy density and intensity of the laser pulse reduced to the wavelength 1 μm.

Because the mean free paths of electrons with energies of several megaelectronvolts and of hard X-rays in matter are substantially greater than the characteristic size of the plasma, the nuclear processes occur, as a rule, outside the plasma, and the plasma itself is a point source of the exciting radiation. Along with electrons and X-ray quanta, nuclear processes can be also induced by ions, which are accelerated in plasma up to energies achieving several hundreds of megaelectronvolts. Having a large cross section of interaction with nuclei, the ions can be directly involved in strong interactions, which is especially important.

In this review, we made an attempt to generalise the experimental data available at present and analysed the possible trends and outlook for further studies. We also considered experimental papers, in which nuclear processes were initiated in the USP plasma at moderate intensities $I_M < 10^{17}$ W cm^{-2}, which are much lower than the intensities corresponding to the so-called relativistic limit $Q_R = I_R\lambda^2 \approx 5.48 \times 10^{18}$ W μm^2 cm^{-2} (λ is the wavelength of laser radiation), when the classical oscillator energy of an electron $\varepsilon_{osc} = (e^2/2\pi m_e c^3)I\lambda^2$ in an external electromagnetic field becomes of the order of its rest energy ($m_e c^2 \approx$ 511 keV). This generation regime is, in our opinion, very interesting for applications because laser setups of such type are comparatively widespread and quite reliable.

2. Heating and acceleration of electrons

Thermal electrons produced in a plasma by ultrashort laser pulses are heated during irradiation up to temperature $T_e \sim 100 - 1000$ eV [6], which is not enough for overcoming the Coulomb barrier of a nucleus and the initiation of nuclear processes. The exclusion is excitation of nuclear levels with energies less than 1–2 keV [7, 8] and fusion reactions [9–11].

The high rate of the energy input to the USP plasma (of the order of 10^{24} J s^{-1} cm^{-3}) results in the nonstationary heating of the plasma. In such a plasma, along with thermal electrons, the so-called hot electron component is formed due to collisionless absorption, which has a non-Maxwellian distribution function of electrons over energy. The consideration of hot electrons becomes important already at moderate intensities, especially in the case of the p polarisation of laser radiation because absorption of this radiation by hot electron components can achieve in this regime 1 %–10 % [12–14].

Because the question of heating of plasma electrons by ultrashort laser pulses of moderate intensities has been considered in a number of reviews [5, 6, 15, 16], we discuss here briefly only the basic features of the formation of a hot electron component. This component is mainly formed due to resonance absorption, vacuum heating, and anomalous skin effect. All these effects take place upon excitation by laser pulses of longer duration as well. Upon excitation by ultrashort laser pulses, a direct interaction of high-intensity laser radiation with a plasma of a solid-state density is realised, and the degree of spreading of the plasma–vacuum interface, which determines the efficiency of various mechanisms of collisionless absorption, becomes to play an important role [17, 18].

A hot electron component is usually characterised by the temperature T_h, although the velocity distribution of electrons proves to be anisotropic and non-Maxwellian, and only the average electron energy has a physical meaning [19]. Fig. 2a shows the typical spectrum of plasma electrons [20]. The numerical calculations [15, 17, 18, 21] and experimental data [22, 23] show that the temperature T_h depends on the parameter $Q = I\lambda^2/Q_R$ as $T_h \propto Q^{0.3-1.0}$ and does not depend on the atomic number A of the target (Fig. 3). The exact value of the exponent is determined by the dominating mechanism of collisionless absorption, i.e., first of all, by the spatial scale of the electron density gradient L. The formation of the hot electron component is accompanied by emission of X-rays. The X-ray spectrum is determined by the energy spectrum of electrons and is located in the region from 3 to 15 keV at moderate intensities [20, 24, 25], while the energy conversion efficiency proves to be proportional approximately to the 1.5 power of the atomic number of the target [26].

As the laser pulse intensity is increased, the increasing fraction of the laser pulse energy (up to 50 % [19, 27]) is spent for the collisionless acceleration of electrons. Already at $Q \sim 1$, the magnetic component $(e/c)[\boldsymbol{v}\boldsymbol{B}]$ (where v is the electron velocity) of the Lorentz force acting on an electron becomes comparable with its electric component $e\boldsymbol{E}$. This results in the acceleration of electrons due to the deviation of their trajectory from a rectilinear one (for linear polarisation of radiation) [28] and also in the acceleration of electrons by a standing wave that appears at the vacuum–plasma interface [29, 30, 31]. In this case, the electron

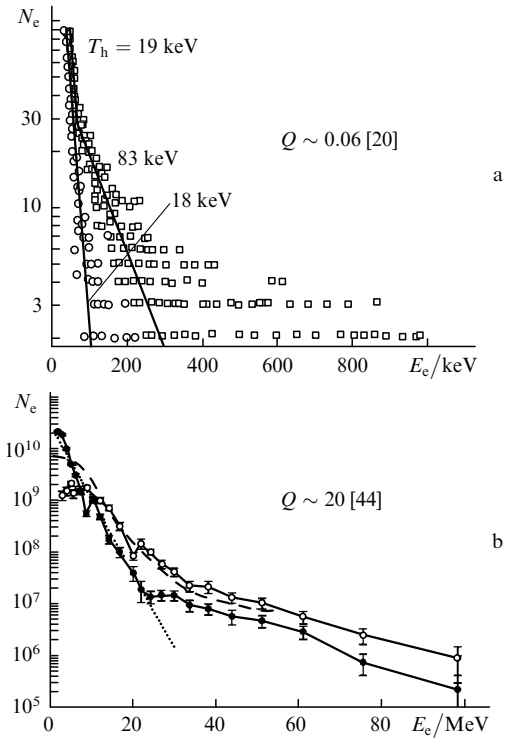

Figure 2. (a) Energy spectra of electrons for $Q = 0.06$ [20] for the high contrast (○) and the contrast 0.1 (□) and their approximation by the straight lines corresponding to temperatures 18, 19, and 83 keV; (b) energy spectra of electrons for two realisations for $Q = 20$ [44] and their approximation for the estimate $T_p \sim 3$ MeV by expression (1) (dotted curve) and the PIC calculation (dashed curve).

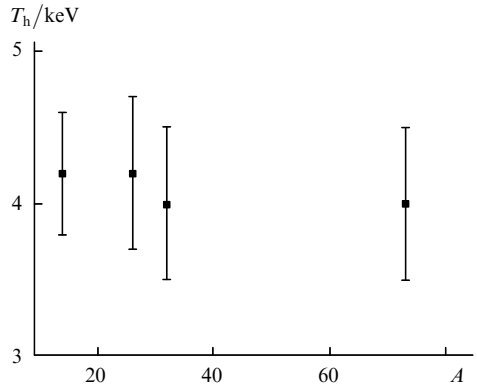

Figure 3. Dependence of the hot-electron temperature T_h of the USP plasma on the atomic number A of the target material.

temperature of the plasma is determined by the gradient of the pondermotive potential

$$T_p = m_e c^2 \left(\sqrt{1 + 4Q} - 1\right) \tag{1}$$

(see approximation in Fig. 2b).

The analysis of the electron spectra of the plasma for relativistic intensities shows (see Fig. 2b) that a fraction of plasma electrons is accelerated to the energies that substantially exceed the estimate by expression (1). This requires the consideration of other possible mechanisms of the electron acceleration.

At relativistic intensities, the contrast of ultrashort pulses that can be achieved in experiments is not sufficient to prevent the laser prepulse to produce a low-density plasma with a characteristic spatial scale of 1–100 μm. Already from the early 1990s, it was known that the interaction of ultrashort laser pulses with a low-density plasma results in a number of new effects such as the relativistic self-focusing and self-channelling (see, for example, [32]), generation of quasi-stationary magnetic and electric fields [33, 34], and the appearance of new mechanisms of electron acceleration.

The first of such mechanisms – the wake-field acceleration in a low-density homogeneous plasma [35] – was considered in a number of papers, including reviews [36, 37]. The low-density homogeneous extended plasma was produced either by exciting a gas with a prepulse [38, 41] or by evaporating thin polymer films with a laser prepulse [42, 43]. The electron energy was 70 MeV [41] when a gas jet was used, the laser pulse duration was $\tau \approx 30$ fs, and Q was ~ 5; and this energy was 30 MeV [43] when a thin-film target was used, the laser pulse duration was $\tau \approx 30$ fs, and Q was ~ 20. The maximum acceleration was achieved at the maximum intensity and plasma parameters corresponding to quasi-resonance excitation of the electron waves with the maximum amplitude $n_e \approx 3 \times 10^{-9}/\tau^2$ (n_e is the electron concentration in the plasma in cm^{-3}; τ is in seconds).

The above acceleration mechanisms were used to explain the acceleration of electrons upon irradiation of solid targets by ultrashort laser pulses of relativistic intensities [44]. It was assumed that electrons were accelerated in expanding plasma produced by a prepulse. However, the calculation performed by the particle-in-cell (PIC) method [45–48] showed that for the plasma density of the order of the critical density, another mechanism, which is related to the transverse betatron oscillations of an electron in the quasi-static field of the plasma channel, is more substantial.

The electron acquires the maximum acceleration when the betatron frequency coincides with the laser radiation frequency in the electron frame of reference. The calculations showed that the electron spectrum is described by the Boltzmann distribution with the temperature equal to 15 MeV for $Q \sim 20$ and extends up to 150 MeV, in accordance with the data [44] (Fig. 2b). It was shown in paper [46] that the electron temperature increases with increasing scaling parameter L and saturates at $L \sim 50$ μm. Note that the parameter L was estimated in paper [44] as 50 μm.

Another mechanism of electron acceleration near the boundary of the high-density plasma was proposed in paper [49] for the case of $L \ll \lambda$. The energy of an electron accelerated in vacuum can be written, in the relativistic regime, as

$$\varepsilon_r \approx 2 m_e c^2 Q, \qquad Q \gg 1. \tag{2}$$

The presence of a sharp plasma–vacuum interface is very important in this model because, similarly to the heating in vacuum, it provides the possibility for the electron accelerated near the interface to leave the region of the electromagnetic field retaining the acquired energy. According to (2), the electron temperature can achieve 20 MeV for $Q \sim 20$. It seems that such a mechanism of electron acceleration can be efficient if the plasma was preliminary compressed by a light pulse.

Therefore, in the case of relativistic laser intensities, electron beams are formed in region (*1*) (Fig. 4) [44, 50], the electrons located in the low-density plasma near the target surface being accelerated most efficiently. Because of the finite size of the focal spot, the electric-field gradient exists across the laser beam as well. As a result, an electromagnetic wave pushes out the electrons from the interaction region by forming a channel with a lower electron density [region (*2*) in Fig. 4]. The main electron flux propagates as a directed beam, which is additionally collimated by the magnetic field of the current of moving electrons [34, 51].

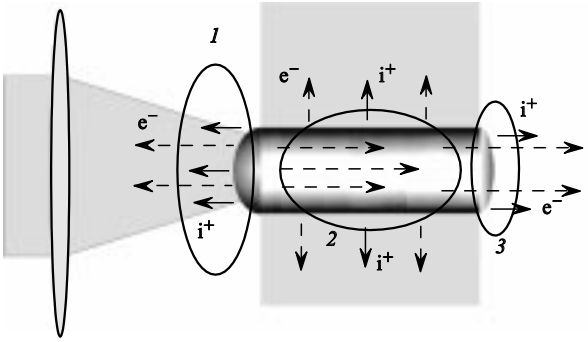

Figure 4. General scheme of the acceleration regions of electrons e^- and ions i^+ in the USP plasma: (*1*) region of acceleration toward the laser beam; (*2*) region of radiation channelling; (*3*) region of acceleration from the rear side of the target.

Hard X-rays indicate the presence of high-energy electrons in the plasma. The authors of paper [52] ($Q \sim 1, \tau \approx 120$ fs) found the presence of electrons with energies up to 1 MeV in the plasma by measuring X-rays. They also noted that a prepulse was necessary for obtaining the efficient generation of hard X-rays, however, the prepulse parameters only weakly affected the generation efficiency.

The hot electron temperature increased up to 10–15 MeV ($Q \sim 20$, $\tau \approx 450$ fs) with increasing intensity of ultrashort laser pulses and the X-ray quantum energy increased up to 100 MeV [44, 53]. In these experiments, a prepulse also produced a low-density plasma with a characteristic spatial scale ~ 50 μm. Because such a situation takes place in most experiments with relativistic ultrashort laser pulses, we will not below mention the presence of a prepulse.

3. Acceleration of ions

In the case of moderate laser-pulse intensities, the ion component of the USP plasma is heated due to electron–ion collisions up to temperatures

$$T_\mathrm{i} \approx \frac{m_\mathrm{e}}{M_\mathrm{i}} T_\mathrm{e} \nu_\mathrm{ei} \tau < 100 \text{ eV},$$

where ν_ei is the frequency of electron–ion collisions and M_i is the ion mass. In this case, the ion energy is insufficient for overcoming the Coulomb barrier by colliding ions or, in the case of the barrierless fusion reactions of the type $^2\mathrm{H(d,n)^3He}$, the cross section of the process is too small to observe the effect.

In the laser plasma, there exists the mechanism of acceleration of ions up to the energies of several tens and hundreds of kiloelectronvolts, which was studied earlier for nanosecond laser pulses [54–57]. The ion acceleration is caused by the gas-dynamic expansion of the electron gas. The plasma ions are ablated predominantly along the normal to the target surface with the velocity of the order of the velocity of sound in the plasma [6]

$$v_\mathrm{s} \approx \left(\frac{3ZT_\mathrm{e}}{M_\mathrm{i}}\right)^{1/2}, \tag{3}$$

where Z is the average charge of plasma ions. The average energy E_i of plasma ions can be estimated assuming that the laser pulse energy absorbed by the plasma is completely converted to the energy of its forward motion. For the energy density of the heating radiation from 1 to 100 kJ cm^{-2} and the plasma-layer thickness of 0.1–1 μm, we obtain $E_\mathrm{i} \sim 10 - 100$ keV, in accordance with the estimate (3) $E_\mathrm{i} \approx ZT_\mathrm{e}$.

The presence of the hot electron component in the plasma results in the acceleration of a fraction of ions up to velocities that substantially exceed v_s. Already at moderate intensities, the electrons accelerated to the energy of 10 keV and above rapidly leave the plasma, thus forming the Coulomb barrier at the plasma-vacuum interface, which produces the accelerating potential for the ions [region (*1*) in Fig. 4]. This field accelerates ions up to significant energies to form a fast ion component with the expansion velocity exceeding the velocity of sound by factors of 5–10. Such ions were oberved earlier in experiments with picosecond and nanosecond laser pulses [54–57], and their appearance was interpreted as the manifestation of the non-Maxwellian velocity distribution of electrons [58].

Measurements of the ions spectrum of the plasma produced by ultrashort pulses of moderate intensity showed that the velocity of the fast component exceeded 10^8 cm s^{-1} both upon channelling radiation in the subcritical plasma [59] and upon irradiation of a solid target [22, 60, 61], the ratio of amplitudes of the fast and thermal components being increased with the laser radiation intensity. The increase in the intensity I and in the energy of hot electrons resulted in the increase in the energy of fast ions approximately proportionally to $Q^{0.5}$ in the range $Q = 0.002 - 2$ [22, 61–63].

The generation of a collimated electron beam in the case of the relativistic intensity of laser radiation leads to the formation of an ion beam, which propagates along the normal to the target surface, both toward the laser beam and inside the target along the low-density channel produced by the radiation [64] [region (*2*) in Fig. 4]. The accelerating Coulomb barrier Ψ can be estimated from the expression [65]

$$\Psi \approx m_\mathrm{e} c^2 \pi \left(\frac{Q\delta r_0}{\lambda}\right)^{1/2}, \tag{4}$$

where δ is the coefficient of conversion to hot electrons and r_0 is the radius of the focal spot. In this case, the ions acquire the energy per nucleon up to $E_\mathrm{i} \approx Z\Psi/A$. Therefore, protons are accelerated most efficiently, while heavy strongly ionised ions acquire the highest energy. For $Q \sim 1$

and $\tau \approx 400$ fs, the proton energy achieves 2–3 MeV [65], for $Q \sim 10$ and $\tau \approx 1000$ fs, the proton energy is 18 MeV [63], and for $Q \sim 20$ and $\tau \approx 500$ fs, this energy is 58 MeV [66]. In paper [63], the energy spectra of ions Pb^{36+}, Pb^{46+}, Al^{13+}, C^{6+}, and H^{+} were also measured for $Q \sim 10$ (Fig. 5). The estimate of the Coulomb barrier for these ions made from Fig. 5 gives $\Psi \approx 6$ MeV (Pb^{36+}), 9 MeV (Pb^{46+}), 11 MeV (Al^{13+}), 15 MeV (C^{6+}), and 10 MeV (H^{+}), which does not contradict, as a whole, to the estimate $\Psi \approx 5$ MeV by expression (4). The ion energy in this acceleration regime considerably exceeds the so-called pondermotive energy

$$E_p \approx ZT_p, \tag{5}$$

which is used for estimating the ion acceleration in a low-density plasma channel [38]. Thus, the estimate by expression (5) for the experimental conditions [63] at $Q \approx 10$ gives the energy 130 MeV for Pb^{48+} ions and 2.7 MeV for protons (see Fig. 5).

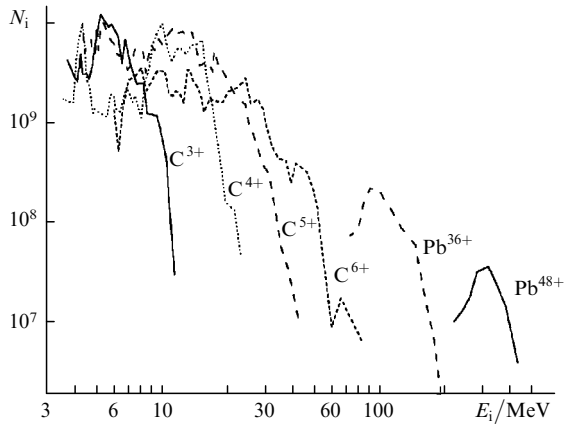

Figure 5. Energy spectra of ions accelerated in the plasma for $Q \sim 10$ [63].

Upon irradiation of thin-film targets, high-energy protons are observed approximately along the normal to the target surface from both its sides [27, 65]. In papers [27, 63, 67], a correlation between the angular and energy spectrum of protons escaping from the rear side of the target was established, the proton energy being increased upon approaching the proton-beam axis. The authors of these papers explained the formation of such a structure by the deviation of protons accelerated at the plasma–vacuum interface inside the target by the magnetic field of the beam of fast electrons propagating at the same direction.

In papers [27, 66], the acceleration of protons was studied for $Q > 20$. As targets, hydrocarbon films and 30° plastic prism irradiated from the hypotenuse side were used. The maximum proton energy was 58 MeV. In the case of a prism target, proton beams with the angular divergence of about 10° were observed along the normal to both rear sides of the prism. This effect was explained in papers [27, 50, 64] by the acceleration of protons on the rear side of the target by the Coulomb field produced by fast electrons generated on the input surface of the target [region (*3*) in Fig. 4]. The scale of the electron-density gradient substantially affects the maximum proton energy. At the blurred input boundary [region (*1*) in Fig. 4], the accelerating field is substantially lower, because it is inversely proportional the density gradient. This results in a substantial increase in the energy of protons observed from the rear surface of the target compared to the energy of protons escaping toward the laser beam.

As the laser radiation intensity is further increased up to $I \approx (M_i/m_e)^2 I_R$ (10^{25} W cm^{-2} for proton plasma), the relativistic mass of the ion becomes equal to the rest mass of the ion [64]. Therefore, the ions can be directly accelerated by the laser field during an optical cycle up to the energy of the order of their rest mass, which is 0.938 GeV for a proton.

Let us discuss the optimal parameters of a laser pulse used for the acceleration of ions in plasma. Expressions (4) and (5) substantially differ from each other, apart from different absolute values of ion energies for the same parameters of the laser pulse, by the wavelength dependences of the maximum energy of ions. According to (4) we have $E_i \propto \sqrt{\lambda}$, whereas it follows from (5) that $E_i \propto \lambda$. The dependence $E_i(I\lambda^2) \propto (I\lambda^2)^{1/2}$ in the range of Q from 0.02 to 10 reported in paper [63] cannot be treated as contradictory to expression (4) because all the data were obtained at $\lambda = 1.053$ μm. The measurements of the energy spectrum of protons for $\lambda = 1.053$ μm and 0.53 μm are presented in papers [65, 68]. The maximum proton energies for $I \sim 2 \times 10^{18}$ W cm^{-2} were $E_{0.53} = 2.5 \pm 0.2$ MeV and $E_{1.05} = 1.5 \pm 0.1$ MeV. The ratio of energies $E_{1.05}/E_{0.53}$ was 1.7 ± 0.2 in the experiment and was 1.4 and 2 according calculation by expressions (4) and (5), respectively. Therefore, the experimental data available do not allow us to determine unambiguously the mechanism of acceleration of ions in the case of relativistic intensities of laser pulses.

Taking into account that expression (4) gives a more realistic estimate of the maximum ion energy E_i, we will assume that

$$E_i \propto (I\lambda)^{1/2} \propto \left(\frac{W}{\tau\lambda}\right)^{1/2}. \tag{6}$$

Here, W is the laser-pulse energy and we assume that the minimum radius of the focal beam is $r_0 \propto \lambda^2$. Therefore, the short-wavelength radiation produces higher-energy ions at $I > I_R$, the peak power W/τ of laser radiation being fixed.

In this connection it is interesting to measure the maximum energy of ions at several wavelengths in a broad range of radiation intensities. The question of the influence of the laser pulse duration on the acceleration of electrons and ions in the solid-state density plasma remains open, at least from the experimental point of view. Such experiments can be performed using modern femtosecond lasers.

4. Interaction with structured media

The properties of the USP plasma can be substantially modified, in particular, its hot-electron and ion temperatures can be increased by using a structured medium consisting of clusters of size $d \sim 1 - 100$ nm. The examples of such a medium are a cluster jet [69, 70] or a nanostructured layer on the target surface [71–75].

Nanocluster jets were used for the first time in paper [69], and then this approach was developed in papers [70, 76, 77]. The studies showed that when the average density of the jet was 10^{19} cm^{-3}, the 100-fs laser pulses interacted with the

cluster microplasma rather than with individual atoms. This leads to deep ionisation of the atoms, the efficient generation of soft X-rays, the appearance of superthermal electrons, fast ions, etc. (see, for example, review [78]).

The influence of I, λ, and τ on the parameters of the plasma produced in a cluster jet was studied in paper [77], and the effect of the cluster size d was investigated in paper [79]. In particular, the mechanism of ion acceleration depends on the size d [80]. For small clusters, the main mechanism is the Coulomb explosion, whereas in large clusters the usual hydrodynamic expansion of the cluster dominates. The numerical calculations showed that ions are accelerated for 50 – 100 fs [81] and their maximum energy amounts to 1 MeV for $I \sim 10^{16}$ W cm^{-2}. The ion energy can be increased by exciting the cluster jet by two pulses, the second pulse being delayed by the time sufficient for the expansion of clusters providing the optimal density of matter [82].

The expansion of individual clusters results in their mutual overlap and causes collisions between accelerated ions. Because the average distance D between the clusters in the interaction region in the jet is $\sim 100 - 1000$ nm, while the size of the interaction region is fractions of millimetre, a homogeneous plasma with the high ion temperature is formed for the time $t_s \approx D/v_s \approx 0.3 - 3$ ps [61]. In such a plasma, fusion reactions can proceed efficiently [10, 83].

Nanostructured targets with the density close to that of a solid were used in experiments [25, 61, 73, 74]. Such targets demonstrate the properties inherent both in cluster jets (the formation of the plasma occurs in each nanocluster separately) and in usual flat targets [84]. Targets made of porous silicon obtained by electrochemical etching of single crystal silicon plates are the most thoroughly investigated nanostructured solid targets. By varying the current density and the concentration of chemical reagents, porous layers of thickness to 10 – 20 μm can be obtained having different morphology and porosity.

For the porosity $P \sim 2 - 3$ (the porosity is the ratio of the density of a uniform material to the mean density of a porous film), submicron channels are formed in a silicon single crystal, while for $P \sim 4 - 7$, a nanostructured porous layer is formed with the mean size of the cluster decreasing from 10 to 2 – 3 nm [25]. The increase in the intensity of soft X-rays emitted by a plasma produced in porous silicon was observed in papers [74, 85].

In paper [25], the dependence of the efficiency of generation of hard X-rays in porous silicon on the porosity P was studied and a direct relation between the mean cluster size and the hot-electron temperature of plasma was found. The maximum temperature T_h equal to 8 – 10 keV for $Q \sim 0.002$ was achieved at the maximum porosity $P \sim 6.6$ and the minimum cluster size $d \sim 2$ nm. It was shown later [61] that the increase in the hot-electron temperature T_h with the intensity I for highly porous silicon occurs substantially faster than the dependence $T_h \sim I^{2/3}$, which is typical for flat targets. The increase in the hot-electron temperature is also reflected in the increase in the expansion velocity of the plasma formed in porous targets [61]. For the porosity $P \sim 6$, the silicon ions with energies up to 2 MeV were observed, whereas in the case of a uniform silicon target, the ion energy did not exceed 1 MeV.

The increase in the temperature and in the number of hot electrons in the USP plasma produced in a dense nanostructured target can be explained by the following. First, due to the developed surface and inner voids, the area of the plasma – vacuum interface increases substantially, which should result in the generation of a great number of hot electrons. In addition, the amplitude

$$X \sim \frac{eE\lambda}{2\pi m_e c}$$

of electron oscillations in the light-wave field becomes comparable to the distance between clusters. For this reason, a fraction of electrons accelerated near the cluster surface does not return back because of collisions with ions from neighbouring clusters. It seems that the 'synchronism' conditions can be satisfied for a fraction of electrons, under which the electrons can be accelerated during the next cycle of the optical field, etc. Finally, no Coulomb barrier appears on the cluster surface, which could prevent the acceleration of electrons on a flat surface: the charge deficiency, which appears upon the removal of a hot electron from the cluster by an external electromagnetic field, is compensated on average due to the arrival of hot electrons from other clusters.

Another variety of solid nanostructured targets is nanosize metal brushes [86], which provide the increase in the yield of soft and hard X-rays [87]. The original approach to the formation of structured targets was demonstrated in paper [61], where a submicron crater produced by a preceding femtosecond laser pulse was used as a target. The studies showed that the hot-electron temperature and the maximum ion energy (Fig. 6) escaping from the silicon target proved to be of the same order of magnitude as for highly porous silicon.

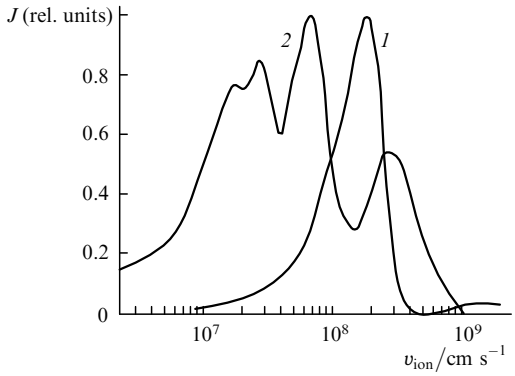

Figure 6. Typical dependences of the ion-current amplitude J on the ion velocity v_{ion} for the uniform (*1*) and laser-modified (*2*) silicon targets.

At present, we are not aware of any studies of solid structured targets at high intensities of laser radiation, although the data obtained allow us to make rather optimistic estimates of the increase in the yield of hard X-rays and in the hot-electron temperature. Thus, as Q is increased by an order of magnitude, up to 0.02, the hot-electron temperature can increase by a factor of 150, achieving 100 – 150 keV compared to 30 – 50 keV for flat targets. For shorter laser pulses, when the time of the structure spreading becomes substantially greater than the time of interaction with the laser pulse, we can expect a further increase in the hot-electron temperature due to the interaction with a sharper cluster boundary.

5. Initiation of nuclear reactions

It seems that the idea of initiating nuclear reactions in the USP plasma was proposed in 1988 [88, 89]. The development of femtosecond laser techniques and the achievement of relativistic intensities of laser pulses pioneered in the mid-1990s the calculations and detailed estimates of the efficiency of a variety of nuclear processes in such a plasma.

The main idea of the PIC calculation performed in paper [90] was the generation of a megaelectronvolt electron beam in the region of the critical plasma density propagating along a laser beam. The authors of paper [90] proposed the 'optimal' model of a target for initiating nuclear processes. The proposed target consisted of a layer of material with a low atomic number (to produce a plasma with critical density), a layer of material with a high atomic number (to decelerate efficiently electrons and generate X-rays), and a layer of deuterium, beryllium or some other material with low threshold of the photonuclear reaction.

The authors of paper [91] proposed to use a laser-plasma channel in a gas-filled capillary for initiating nuclear reactions in the capillary walls by radially accelerated ions and electrons. This scheme allows one to obtain a great number of accelerated particles, up to 10^{13}, according to the estimate of the authors, providing efficient initiation of fusion, photonuclear, and other reactions. The energies of electrons and ions were calculated in paper [91] by expression (5), which resulted in the overestimation of reaction thresholds up to 10^{20} W cm^{-2} and above.

The observation of photoexcitation of nuclei by radiation from the USP plasma was reported for the first time at the IQEC'98 conference by researches at the Lawrence Livermore National Laboratory (USA) [92]. Later, the results of these studies were described in a series of papers [44, 53, 93], where the authors observed activation of nuclei by the USP plasma radiation, uranium fission, generation of powerful neutron fluxes, etc. The experiments were performed for $Q > 20$ and $\tau \approx 400$ fs, which provided the production of electrons and gamma quanta with energies up to 100 MeV.

The target consisted of a massive copper cylinder with gold plates. A variety of photonuclear reactions were observed in experiments with thresholds from 8 to 11 MeV (Fig. 7): $^{197}\mathrm{Au}(\gamma,\mathrm{n})^{196}\mathrm{Au}$, $^{63}\mathrm{Cu}(\gamma,\mathrm{n})^{62}\mathrm{Cu}$, $^{65}\mathrm{Cu}(\gamma,\mathrm{n})^{64}\mathrm{Cu}$, etc. In the same experiments, but with a target with an additional uranium plate, a broad spectrum of photofission fragments of ^{235}U was observed. The authors of paper [44] also noted that the parameters of the high-energy gamma quanta could be estimated from the mass distribution of fission fragments. A series of studies on photoexcitation of nuclei for $Q \sim 4$ and $\tau \approx 1$ ps was simultaneously performed at the Rutherford Laboratory [94–96]. It was shown in paper [94], by measuring the activity of irradiated samples oriented at different angles with respect to the normal to the target surface, that radiation in the range from 100 keV to 1 MeV propagated almost along the normal to the target surface within a cone of angle 30°. This fact was explained by numerical calculations of the features of acceleration of electrons in the case of relativistic intensities [30, 31, 49], which was accompanied by the formation of a collimated electron beam propagating along the normal to the target surface.

One of the possible applications of the activation of nuclei by radiation from the USP plasma is the recovery of isotopes for medical applications and calibrated radiation sources. However, this method is economically unprofitable when hybrid single-pulse lasers with neodymium glass amplifiers are used. Thus, the estimate showed that more than 10^6 of 25-J laser pulses are required for the ^{88}Y isotope recovery with the activity of 1 MBq in the reaction $^{89}\mathrm{Y}(\gamma,\mathrm{n})^{88}\mathrm{Y}$ (the half-life of the ^{88}Y isotope with emission of quanta with energies of 0.899 and 1.836 MeV, which is often used for calibration of detectors, is 108 days). The recovery efficiency can be increased by using a femtosecond Ti:sapphire laser with a kilohertz pulse repetition rate at $Q \sim 1$.

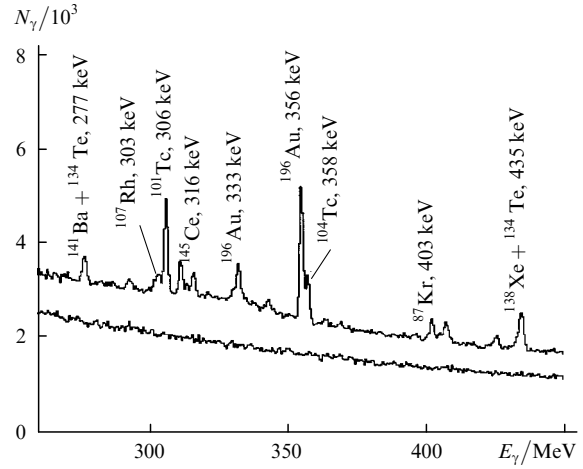

Figure 7. Spectra of nuclear gamma radiation of the USP plasma for $Q > 20$ [44] (the lower curve was obtained in the absence of laser radiation).

A 60-fs laser system with a pulse repetition rate of 10 Hz was used in paper [97], where a chain of reactions $^{9}\mathrm{Be}(\gamma,\mathrm{n})2\alpha \rightarrow (^{197}\mathrm{Au},\mathrm{n})^{198}\mathrm{Au}$ was studied. A low energy threshold (1.67 MeV) of the first reaction allowed the operation near the relativistic limit $Q \sim 1$ at the electron temperature of 700 keV. To increase the efficiency of generation of gamma radiation, a tantalum disc was used as a target and a Be plate was placed at a distance of 4.5 cm from the target. The neutrons obtained in the $^{9}\mathrm{Be}(\gamma,\mathrm{n})2\alpha$ reaction were decelerated with the help of a polyethylene sphere with a ^{197}Au disc located at its centre. The thermal neutron-capture reaction $^{197}\mathrm{Au} + \mathrm{n} \rightarrow {}^{198}\mathrm{Au}$ was detected by emission of 411-keV gamma quanta.

It has been noted in paper [98] that positrons can be produced upon scattering of megaelectronvolt electrons by atoms in a layer of a material with a high atomic number. The generation of positrons upon the interaction of high-energy electrons with a target was considered in more detail in papers [90, 99]. It was shown that of the two possible channels of positron generation – a direct channel and a channel involving the generation of a gamma quantum – at the electron energy of the order of 10 MeV, which is typical for the USP plasma, the latter channel is more efficient (the cross section of the process for a 10-MeV electron is ~ 10 μb). Positrons were experimentally observed for the first time in paper [100] for $Q > 20$ using an Au target (the experimental conditions were similar to those used, for example, in paper [27]). In paper [101], fast electrons with energy up to 5 MeV were generated in a plasma channel in a He jet at $Q \sim 2.5$ and $\tau \approx 130$ fs, while positrons were obtained upon irradiation of a lead target by an

electron beam. In each laser pulse, up to 10^6 of 2-MeV positrons were generated, which corresponds to the activity above 10^7 Bq. It is important that the source activity can be substantially increased by increasing the laser pulse repetition rate from 10 Hz to several kilohertz.

Nuclear reactions can be efficiently initiated by light-ion beams, which appear in the laser plasma because the thresholds of the (p, n) reaction are, as a rule, substantially lower than those of photonuclear reactions, whereas the corresponding cross sections are an order of magnitude higher. In addition, the mean free path of ions in a matter is substantially smaller than that of gamma quanta, which allows one to use thin samples, thereby obtaining the higher activity. Thus, a 30-MeV proton beam was generated in paper [102] by focusing a 1-ps laser pulse with $Q \sim 5$ on targets made of graphite, aluminium, titanium, glass, and polyethylene. The nuclear reactions $^{63}\mathrm{Cu}(\mathrm{p,n})^{63}\mathrm{Zn}$, $^{11}\mathrm{B}(\mathrm{p,n})^{11}\mathrm{C}$, $^{16}\mathrm{O}(\mathrm{p},\alpha)^{13}\mathrm{N}$, and $^{13}\mathrm{C}(\mathrm{p,n})^{13}\mathrm{N}$ were studied. The laser pulse energy up to 60 J provided a high activity of the sample obtained (up to 140 kBq).

Note that such isotopes as $^{11}\mathrm{C}$, $^{13}\mathrm{N}$, $^{15}\mathrm{O}$, and $^{18}\mathrm{F}$ are widely used in nuclear tomography based on the detection of positrons [103]. According to estimates performed in paper [102], the radiation load on patients can be substantially reduced by using laser-plasma sources of protons: up to 80 kBq of the $^{18}\mathrm{F}$ isotope can be obtained per laser pulse and up to 150 MBq by using laser systems with a pulse energy of 1 J and a pulse repetition rate of 10 Hz.

In paper [68], a tabletop femtosecond laser system was used. A target representing a 1-μm thick layer of deuterated polystyrene on a 6-μm thick mylar substrate was irradiated by 400-fs laser pulses with a repetition rate $F = 10$ Hz and $Q \sim 1$. On the rear side of the target, a boron sample enriched with the $^{10}\mathrm{B}$ isotope (the enrichment degree was 90 %) was placed. The irradiation of the sample by deuterium ions initiated the $^{10}\mathrm{B}(\mathrm{d,n})^{11}\mathrm{C}$ reaction with the sample activity of 74 Bq immediately after the laser pulse. Because the lifetime of the $^{11}\mathrm{C}$ isotope is ~ 7 min, the sample activity was increased to 740 Bq for $F = 10$ Hz. Note that when the deuterated layer was placed on the rear side of the target, the induced activity proved to be lower than the detection threshold. This means that for $Q < 1$, the ions are accelerated at the plasma-vacuum interface rather than on the rear side of the target.

Heavy ions also can excite nuclear levels, fusion reactions, etc . [4]. The key parameter in this case is the Coulomb threshold B (in MeV) corresponding to a collision of an ion with the charge Z_i with a nucleus with the charge Z_n and radius R_n [4]:

$$B \approx Z_\mathrm{i} Z_\mathrm{n} e^2 / R_\mathrm{n} = Z_\mathrm{i} Z_\mathrm{n} A^{-1/3}.$$

When the ion energy is lower than the Coulomb threshold B, the selective excitation of rotational nuclear spectra is possible. Upon a collision of two uranium ions and their approach to the critical distance of 35 fm (the required ion energy exceeds 600 MeV upon a head-on collision [4]), quasi-atoms can be produced with a double nucleus and a charge above 170. Note that the energy of Pb^{46+} ions equal to 460 MeV has been already achieved in paper [63] for $Q \sim 10$. When the energy of nuclei exceeds the Coulomb threshold, apart from the electromagnetic interaction, the nuclear interaction is possible, fusion reactions can occur, etc.

6. Excitation of nuclear levels

Electrons and X-rays emitted by the USP plasma can not only initiate nuclear reactions but also excite nuclear levels. These processes are of interest for a number of promising applications such as the isotope separation [104, 105] and the creation of population inversion [106, 107]. In particular, X-rays emitted by the USP plasma can be efficiently used for excitation of metastable isotopes to the closely spaced level accompanied by its decay to the ground state. This was realised in paper [108], where the metastable level of $^{178}\mathrm{Hf}$ with the energy of 2.446 MeV and the lifetime of 31 year was excited with a cw X-ray tube.

To our knowledge, no experiments have been performed in this field at relativistic intensities. However, as noted earlier, the hot-electron temperature was from 3 to 10 keV already for moderate intensities, which is sufficient for direct excitation of low-lying nuclear levels of both stable and metastable isotopes [8] (we call the nuclear levels with energy $\varepsilon_\gamma < 20$ keV the low-lying nuclear levels). The standard methods of nuclear spectroscopy of such levels are based on the indirect population via the states with energy $\varepsilon_\gamma > 100$ keV using electron and ion accelerators [109, 110] or on the direct photoexcitation using synchrotron radiation sources [111, 112].

Note that the parameters of low-lying nuclear levels are often unknown (even when the ground state of a nucleus is stable) (see, for example, Table 1). For metastable isotopes, the situation when a number of parameters are unknown is encountered even more often. An important positive factor is that the low-lying nuclear levels in a plasma are excited 'instantly' because the relation $\tau_\gamma \gg \tau_\mathrm{p}$ is satisfied (τ_γ is the total lifetime of the excited state and τ_p is the lifetime of a hot dense plasma).

Table 1. Parameters of low-lying nuclear levels of stable isotopes

Element	ε_γ/keV	M	τ_γ/ns	Π	β
$^{201}_{80}\mathrm{Hg}$	1.556	1/2−	1 − 10	M1 + E2	$(2-5) \times 10^4$
$^{181}_{73}\mathrm{Ta}$	6.238	9/2−	6050	E1	70.5
$^{169}_{69}\mathrm{Tm}$	8.4103	3/2+	4.08	M1 + E2	285
$^{83}_{36}\mathrm{Kr}$	9.396	7/2+	147	M1 + E2	17.09
$^{187}_{76}\mathrm{Os}$	9.746	3/2−	2.38	M1(+E2)	264
$^{45}_{21}\mathrm{Sc}$	12.40	3/2+	3.18×10^6	(M2)	632
$^{73}_{32}\mathrm{Ge}$	13.275	5/2+	2950	E2	1120
$^{57}_{26}\mathrm{Fe}$	14.4129	3/2−	98.3	M1 + E2	8.56
$^{151}_{63}\mathrm{Eu}$	21.541	7/2+	9.6	M1 + E2	28
$^{161}_{66}\mathrm{Dy}$	25.6515	5/2−	29.1	E1	2.35
$^{201}_{80}\mathrm{Hg}$	26.269	5/2−	0.630	M1 + E2	76.7

Notes: ε_γ is the excitation energy; M is the moment and parity; $\tau_\gamma = [\Gamma_2(1+\beta)]^{-1}$ is the total lifetime; $\beta = P_\mathrm{e}/P_\gamma$ is the internal conversion coefficient; Γ_2 is the radiative width of a nuclear transition; $P_{\mathrm{e},\gamma}$ is the probability of the internal electron conversion decay and gamma decay, respectively; Π is the transition multiplicity.

The possibility of excitation of low-lying nuclear levels in the laser plasma has been discussed over twenty years [104, 113, 114]. Experimental attempts to use the low-density laser plasma were scarce [115, 116] and unsuccessful [117]. The main problems are related to the low efficiency of

excitation by nanosecond laser pulses because of a low electron temperature of the plasma and its low density. As shown in papers [7, 118], the USP plasma is free from these disadvantages and it has at the same time a sufficiently high electron temperature and the nuclear density that is close to that of a solid.

The gamma decay of the low-lying nuclear level of the stable ^{181}Ta isotope with energy 6.238 keV was observed for the first time in papers [8, 119]. The isotope was excited in a dense hot plasma produced by 200-fs laser pulses with $Q \sim 0.005 - 0.01$ (Fig. 8). A comparison of the experimental and theoretical results showed [119, 120] that excitation occurred not only inside the plasma but also in the region with linear dimensions of the order of the extinction length for X-rays. At the same time, the excitation probability, which was estimated from the experimental data, is approximately an order of magnitude higher than the calculated probability. In principle, such a situation is typical for spectroscopy of low-lying nuclear levels [114, 121] and reflects the necessity of improving both experimental methods and theoretical models.

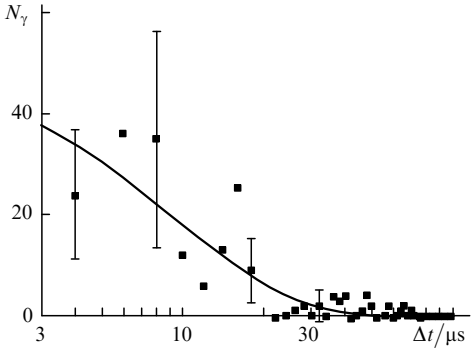

Figure 8. Dependence of the number N_γ of detected gamma quanta emitted from the ^{181}Ta target on the delay time Δt with respect to the exciting laser pulse [119].

The low-lying nuclear levels in the laser plasma can be excited via different channels, both nuclear–electronic and nuclear–photonic [7, 118]. The inelastic scattering of electrons by nuclei [117, 122], inverse internal electron conversion [123], and excitation by X-rays emitted by the plasma [124] make the main contribution. The latter process dominates in the USP plasma.

The efficiency of excitation of nuclei in the USP plasma can be calculated using a two-level model of nuclear transitions. This is explained by the fact that, first, the energy spectrum of electrons and X-rays in the plasma is overlapped, as a rule, only with one of the nuclear levels. Second, because the pumping is incoherent, the interference effects are almost excluded. Additional simplifications appear because the excitation time τ_p is short compared to the longitudinal and transverse relaxation times ($\Gamma_{1,2}\tau_p \ll 1$), and the number n_2 of excited nuclei is small compared to their total number in the irradiated region. Then [125],

$$n_2 = n_0 \frac{2\pi}{\hbar^2} \iint \left\{ \frac{2\Gamma_2 |H'_{12}(\omega)|^2}{\Gamma_2^2 + (\omega - \omega_0 + \Delta)^2} - \frac{\Gamma_2 \left[H'_{12}(\omega_0 + \Delta) H'^{*}_{12}(\omega) + H'_{12}(\omega) H'^{*}_{12}(\omega_0 + \Delta) \right]}{\Gamma_2^2 + (\omega - \omega_0 + \Delta)^2} \right. \tag{7}$$

$$\left. + \mathrm{i} \frac{(\omega - \omega_0) \left[H'_{12}(\omega_0 + \Delta) H'^{*}_{12}(\omega) - H'_{12}(\omega) H'^{*}_{12}(\omega_0 + \Delta) \right]}{\Gamma_2^2 + (\omega - \omega_0 + \Delta)^2} \right\}$$

$$\times g(\Delta) \mathrm{d}\Delta \mathrm{d}\omega,$$

where n_0 is the isotope concentration in the plasma volume; Δ is the detuning from the centre of the transition line; $g(\Delta)$ is the profile of an inhomogeneous line broadened by the factors considered above; $H'_{12}(\omega)$ is the Fourier component of the matrix element of the Hamiltonian of interaction of a nucleus with external electromagnetic fields and charges produced in the plasma; ω_0 is the nuclear transition frequency; and Γ_2 is the radiative width of the nuclear transition. Note that, if the exciting pulse duration becomes comparable to the transverse relaxation time ($\Gamma_2\tau_p \gtrsim 1$) but is still shorter than the longitudinal relaxation time ($\Gamma_1\tau_p \ll 1$), then expression is further simplified: in this case, only the first term can be kept in the braces).

As mentioned in previous sections, the high-frequency part of the X-ray spectrum of the plasma is mainly determined by inelastic scattering of hot electrons by plasma ions. The spectral densities of the longitudinal and transverse pump fields can be related to the spectral dependences of the charge $\rho_z(\boldsymbol{r}, t)$ and current $\boldsymbol{j}_z(\boldsymbol{r}, t)$ densities for electrons and ions with different ionisation degrees $z = \pm 1, +2, +3, \ldots$. If a particle undergoes inelastic collisions at random instants of time t_i and the duration τ_0 of each collisions depends on the particle velocity $v_i = v(t = t_i)$ directly before the collision as $\tau_0^{-1} = \alpha v$, then

$$\langle A^*(\omega) A(\omega') \rangle = \sqrt{\pi} \left(\frac{e}{2\pi c} \right)^2 \sum_{i=0}^{N} \int_{t_i}^{t_{i+1}} \frac{v^2(t)}{R^2(t)} \exp(\mathrm{i}\zeta t) \mathrm{d}t$$

$$\times \left\langle \tau_0 \exp\left(-\frac{\Omega^2 \tau_0^2}{4} \right) \right\rangle, \tag{8}$$

where N is the number of collisions; $\boldsymbol{R}(t)$ is the radius vector of an electron at the instant of time t; and $\zeta = \omega - \omega'$; $\Omega = (\omega + \omega')/2$. It is reasonable to assume that the duration τ_0 of each collision is much shorter than the mean free time $t_0 = \langle t_{i+1} - t_i \rangle$, and the distribution over random velocities v_i coincides with the velocity distribution of particles in the plasma and is described by the Maxwell distribution. By introducing the spectral density $\mathrm{d}I = (c/4\pi)\langle E^2(t) R^2(t) \rangle \mathrm{d}o = \int I(\omega) \mathrm{d}\omega \mathrm{d}o$ of the radiation intensity $I(\omega)$ in the frequency interval $\mathrm{d}\omega$ and the solid angle $\mathrm{d}o$, we obtain from (8)

$$I(\omega) = \frac{e^2 \langle v^2 \rangle \omega^3}{(2\pi\alpha v_0)^2 c^3} K_1\left(\frac{\omega}{\alpha v_0} \right), \tag{9}$$

where $K_1(x)$ is the modified Bessel function;

$$\langle v^2 \rangle = \frac{1}{t_0} \int_0^{t_0} v^2(t) \mathrm{d}t$$

is the square of the particle velocity averaged over the mean free time t_0; and $v_0 = (2kT_e/m_e)^{1/2}$ is the most probable velocity of the Maxwell distribution. The dependence $I(\omega)$ is shown in Fig. 9. The dependence $I(\omega)$ resembles qualita-

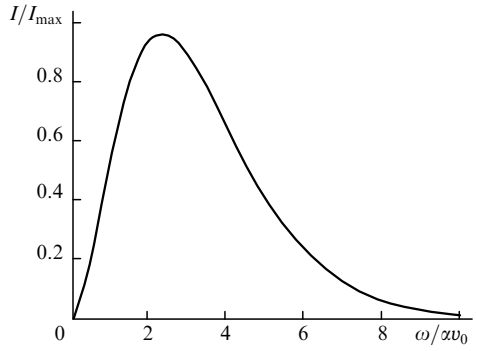

Figure 9. Spectral dependence of the normalised intensity I/I_{max} of X-rays emitted by the laser plasma calculated by expression (9)

tively that for the blackbody radiation, however, the spectral density of the plasma radiation has a maximum at the frequency $\omega_m = 2\alpha v_0$, which is equal to the inverse mean collision time of particles in the plasma.

Let us estimate the efficiency of excitation of the low-lying nuclear level with the energy 10 keV and the lifetime $\tau_\gamma = 10$ ns. According to expression (7), if the level is coupled with the ground level by the electric dipole transition, the excitation efficiency is determined by the expression

$$\eta = \frac{n_2}{n_0} = \frac{4\pi}{\hbar^2}|d_{20}|^2|E(\omega_0)|^2, \tag{10}$$

where d_{20} is the nuclear transition dipole moment. Let $\tau_p \approx \tau$, then $E(\omega_0) = (1/2\pi)\int_0^{\tau_p} E_0 dt$ and $\eta = |\Sigma|^2/\pi$, where $\Sigma = d_{20}\int_0^{\tau_p} E_0(t)dt/\hbar$ is the pulse area. Therefore, we see that although expression (10) was derived using the perturbation theory, it gives a rather realistic estimate of the excitation efficiency even for $\eta \approx 1$. As the characteristic scale for the field of X-rays emitted by the plasma, it is convenient to use the field strength E_m at which the total population inversion is achieved ($\eta = 1$). We see that, if the emission spectrum of the plasma is homogeneous within the linewidth of the nuclear transition, then the efficiency of excitation of nuclei integrated over the spectrum is virtually independent of the level width. We can readily obtain from (10) that for $\eta = 1$ the field strength $E_m = 10^9$ V cm^{-1}.

On the other hand, we obtain from (9)

$$|E_0|^2 = \left(\frac{\omega}{\alpha v_0}\right)^3 K_1\left(\frac{\omega}{\alpha v_0}\right)\frac{N}{\pi r_0^2}\frac{3e^2 T_e \omega_m \Delta_D}{m_e c^4},$$

where Δ_D is the Doppler width of the transition; $r_0^2 \approx \langle R^2(t)\rangle$; N is the number of collisions of electrons during the plasma lifetime, which can be estimated as $N = Zn_0 V\tau_p \nu_{ei}$; V is the volume of the excitation region. By substituting into the latter expression the typical values of parameters for the laser radiation intensity $I \sim 10^{16}$ W cm^{-2}, we obtain $\eta = |E_0/E_m|^2 \approx 10^{-10} - 10^{-11}$. We can calculate similarly the spectrum of the longitudinal electromagnetic field, which is responsible for the collision or Coulomb excitation of nuclei.

The low-lying nuclear states decay predominantly via internal electron conversion and gamma decay. The decay kinetics may substantially depend on the processes proceeding upon ionisation, recombination, and cooling of the plasma. Indeed, the ionisation of atomic shells can result in a complete or partial suppression of internal electron conversion, which is the main channel of the decay of an excited nuclear level [110, 126]. This, in turn, leads to the increase in the lifetime of the excited nuclear state, the appearance of new decay channels of the electronic bridge type [127, 128], etc. The numerical analysis showed [129] that the degree of ionisation of ions required for the prohibition of internal electron conversion can be obtained in the mercury plasma upon excitation of the low-lying 1.561-keV level of the ^{201}Hg isotope.

7. Population inversion schemes for nuclear transitions

The study of low-lying nuclear levels of metastable isotopes substantially expands the field of investigations. One of the problems can be a search for candidates suitable for the production of population inversion at nuclear transitions.

One can see from Table 1 that the lifetime of low-lying nuclear levels greatly exceeds that of the plasma, so that the population inversion can be produced during the plasma lifetime. At the same time, to obtain the population inversion for the nuclear level with energy ~ 10 keV, when the nuclear density is close to the density of a solid, the X-ray intensity within the nuclear transition band should be $\sim 10^{16}$ W cm^{-2}, which corresponds to the laser radiation intensity $I > 10^{21}$ W cm^{-2}. For such intensities, the electron temperature exceeds 10 MeV and it strongly differs from the optimal temperature $T_h \approx \varepsilon_\gamma$ for the energy range of transitions under study.

From the point of view of observation of stimulated emission at nuclear transitions, the isotopes presented in Table 1 can be divided into two groups. In the case of nuclei with the high conversion coefficient at the transition to the ground state (^{201}Hg, ^{181}Ta, ^{169}Tm, ^{187}Os, ^{73}Ge), one can hope to obtain generation only in a plasma layer containing ions with a high degree of ionisation, because the conversion coefficient can be completely or strongly suppressed in this case. In the case of isotopes with a relatively low conversion coefficient (^{83}Kr, ^{57}Fe, ^{161}Dy), it is preferable to attempt to produce inversion in a solid sample. Such an inversion can be achieved, for example, using a multicomponent target consisting of a metal foil emitting X-rays and an active body, which has no thermal contact with the foil. This substantially decreases the Doppler broadening and allows, in principle, the development of schemes of the Mössbauer gamma laser.

When ultrashort laser pulses with $Q \approx 1$ are used, the hot-electron temperature achieves several hundreds of kiloelectronvolts, providing the possibility for excitation of higher-lying nuclear levels. Consider nuclei of isotopes ^{73}Ge, ^{83}Kr (Table 2), and ^{107}Ag, ^{109}Ag, ^{119}Sn. These nuclei have a number of common features. First, the radiative decay of the first two excited levels is cascade, i.e., the gamma transition from the second excited level occurs to the first level, whereas the transition to the ground state is forbidden. Second, all the isotopes have a long-lived isomeric state with the lifetime of the order of 1 s and longer. Third, these transitions have a rather high electron conversion coefficient.

In the scheme for producing the population inversion under study, the temperature T_h should provide cascade

Table 2. Low-lying nuclear levels of isotopes for the three-level lasing scheme.

Element	ε_γ/keV	M	τ_γ/ns	γ transition			β
				Π	I_γ	ε'_γ/keV	
	0	9/2+					
	13.275	5/2+	2950	E2	100	13.275	1120
$^{73}_{32}$Ge	66.716	1/2−	0.499×10^9	M2	100	53.440	8.67
	68.752	(7/2)+	1.74			55.42	
	68.752	(7/2)+	1.74	M1 + E2	100	68.752	0.227
	0	9/2+					
$^{83}_{36}$Kr	9.396	7/2+	147	M1 + E2	100	9.396	17.09
	41.543	1/2−	1.83 h	E3	100	32.1473	2035

Notes: ε'_γ is the gamma transition energy; I_γ is the gamma transition intensity. Other notation as in Table 1.

Table 3. Low-lying nuclear levels of isotopes for the four-level lasing scheme. Notation as in Tables 1 and 2.

Element	ε_γ/keV	M	τ_γ/ns	γ transition			β
				Π	I_γ	ε'_γ/keV	
	0	5/2+					
	83.36720	7/2+	0.793	M1 + E2	100	83.36717	3.82
$^{153}_{63}$Eu	97.43103	5/2−	0.198	E1	0.12	14.06383	11.2
	97.43103	5/2−	0.198	E1	100	97.43100	0.307
	103.18016	3/2+	3.85	E2		19.81296	3290
	103.18016	3/2+	3.85	M1 + E2	100	103.18012	1.72
	0	3/2−					
	60.0087	5/2−	0.193	M1 + E2	100	60.0086	9.36
	86.5460	5/2+	6.50	E1	1.03	26.533	2.00
$^{155}_{64}$Gd	86.5460	5/2+	6.50	E1	100	86.545	0.434
	105.3109	3/2+	1.16	M1 + E2	0.23	18.764	375
	105.3109	3/2+	1.16	E1	6.27	45.2972	0.445
	105.3109	3/2+	1.16	E1	100	105.305	0.256
	0	3/2−					
	54.533	5/2−	0.130	M1 + E2	100	54.548	12.40
$^{157}_{64}$Gd	63.917	5/2+	460	E1	7.1	9.365	30.8
	63.917	5/2+	460	E1	100	63.929	0.971
	115.717	7/2+		M1 + E2	100	51.834	14.61
	0	3/2−					
	30.814	9/2−	5.8 h	M3 + E4	100	30.814	324000
$^{189}_{76}$Os	36.202	1/2−	0.53	M1 + E2	100	36.202	21.0
	69.537	5/2−	1.62	E2	0.19	33.335	739
	69.537	5/2−	1.62	M1 + E2	100	69.537	8.48

excitation of the second nuclear level by X-rays emitted from the plasma or its direct excitation due to inelastic electron scattering. The expanding plasma containing highly ionised ions is deposited on a surface where the ions are completely neutralised. During the lifetime of isotopes ^{73}Ge, ^{83}Kr, and ^{119}Sn in the second excited state, a rather large number of nuclei can be produced in the isomeric state. The ions formed due to the conversion decay at the $2 \to 1$ transition are pulled out by a focusing electric field and are deposited on a substrate, where the active body of a gamma laser is formed. The ^{83}Kr isotopes are most promising for the creation of a gamma laser using the scheme considered, because their second excited state has a low energy and an optimal lifetime for producing a great number of isomers. A long lifetime of silver isotopes ^{107}Ag and ^{109}Ag in the first excited state gives promise that it is possible to produce the active body of a gamma laser in the form of a crystalline film on a cooled crystalline substrate.

The latter method for producing the population inversion can be also used for the development of four-level lasing schemes (Table 3). In this case, nuclei at the level 2 are selected due to the conversion decay at the $3 \to 2$ transition, while the lasing should occur at the $2 \to 1$ or $2 \to 0$ transition. Among the isotopes having the required energy level diagram are $^{153}_{63}$Eu, $^{155}_{64}$Gd, $^{157}_{64}$Gd, and $^{189}_{76}$Os. A substantial difference of the four-level scheme from the three-level scheme is, for example, the fact that the third excited level of isotopes ^{153}Eu, ^{155}Gd, and ^{189}Os is coupled with the ground state of the nucleus by a radiative transition having a low conversion coefficient. Therefore, the nucleus can be excited to the third level in a multicomponent target by filtered X-rays emitted by the laser plasma, which excludes the necessity to neutralise plasma ions. Another advantage of the four-level scheme with the $2 \to 1$ lasing transition (^{153}Eu and ^{155}Gd isotopes) is that this scheme is insensitive to the presence of nuclei in the ground state in the active region of the gamma laser. This substantially decreases technological requirements imposed on the process of preparation of the active region.

Among stable isotopes with low-lying nuclear levels with energies less than several hundreds kiloelectronvolts there are isotopes that permit the use of three- and four-level lasing schemes, which are typical for the visible range. The first five excited levels in the ^{161}Dy isotope are coupled by radiative transitions with the ground state and, therefore, they can be excited by laser plasma X-rays. The transitions $2 \to 1$ ($\varepsilon_\gamma = 18.15$ keV), $3 \to 1$ (49.92 keV), $4 \to 2$ (56.64 keV), $5 \to 2$ (56.235 keV), and $5 \to 1$ (77.414 keV) are promising for lasing. It seems that the most promising are the transitions terminating on the second excited level because the lifetime of this level (0.83 ns) is 35 times shorter than that of the first excited state.

The ^{171}Yb isotope is of great interest for the development of lasing schemes for nuclear transitions because its third excited level with energy of 95.272 keV has a lifetime of 5.25 ms. This level is coupled by the radiative transition only with the second excited level wit energy of 75.878 keV. However, the third level can be excited due to inelastic electron – ion and ion – ion collisions or due to the radiative transition via the fourth excited level with energy of 122.418 keV. The latter level is coupled with the third level by an intense radiative transition with the multiplicity E1.

The three- and four-level schemes of gamma lasers proposed above can be used in experiments on detection of stimulated gamma radiation. To perform such experiments, a rather small amount of excited nuclei is sufficient. Consider, for example, the ^{83}Kr isotope. After excitation in the laser plasma and termination of recombination, atomic gas, which contains, in particular, atoms with nuclei in the second excited state, can be cooled and placed in an atomic trap. This can be easily realised due to a long lifetime of the second excited state (1.83 h). The atoms that underwent the conversion decay will escape from the atomic trap due to recoil upon emission of an electron. The ions formed in this

process can be easily placed in an ion trap. The detection of stimulated radiation can be based on the measurement of the temporal or spectral decay parameters of an ensemble of excited nuclei found in the ion trap at equal numbers of nuclei.

8. Initiation of fusion reactions

One of the promising applications of the USP plasma can be the creation of a source of ultrashort pulses of fast neutrons. Note that the Lawson criterion [4] cannot be fulfilled for the USP plasma, which means that a self-sustained fusion reaction cannot be initiated in such plasma. Although some fusion reactions have no the energy threshold, their cross section very strongly depends (at low energies, exponentially) on the energy of colliding nuclei, reaching a maximum at 1 MeV for the DD reaction and at ~ 100 keV for the DT reaction [130]. When the energy of nuclei is less than 100 eV, the cross section for the DD reaction is so low ($\sigma_{dd} < 10^{-38}$ cm^2) that the neutron yield N_n for typical experimental parameters (the plasma volume) is also low [11]:

$$N_n \approx \frac{N_d}{2} \langle \sigma v \rangle_{dd} n_d \ll 1, \qquad (11)$$

where N_d and n_d are the number of accelerated deuterons and the deuterium concentration in the plasma.

The ion temperature of the USP plasma does not exceed 50 eV, and for the fusion reaction to proceed efficiently and for obtaining a sufficient number of neutrons, the plasma ions should be additionally heated or accelerated up to energies of several kiloelectronvolts. Such acceleration can be obtained by irradiating deuterated targets by pulses with relativistic intensities: deuterons can be accelerated like protons inside the target up to energies of several megaelectronvolts.

For example, the neutron yield N_n in the polystyrene target plasma produced by 1.5-ps pulses with $Q \sim 15$ [131] was 7×10^7 neutron pulse^{-1} for $W \sim 20$ J. To generate neutrons by 160-fs pulses with $Q \sim 0.3$ [132], a prepulse was used, which contained up to 15 % of the main pulse energy and was ahead of the main pulse by 300 ps. The authors of paper [132] assumed that deuterons were mainly accelerated in the radial direction due to the Coulomb explosion in a plasma channel. A higher neutron yield ($N_n \sim 10^4$ neutron pulse^{-1}) was recently obtained [133] using 50-fs laser pulses with $Q \sim 0.3$ and a low contrast. The study of angular and energy spectra of neutrons revealed two neutron components corresponding to the radial acceleration of deuterons and their acceleration along the laser-beam axis inside the target.

Another mechanism of ion acceleration was used in paper [134], where experiments were performed using 300-fs laser pulses with $Q \sim 2.5$ and a contrast up to 10^{12}. The study of the angular dependences of the neutron yield showed that ions were accelerated at the plasma–vacuum interface predominantly along the laser-beam axis. In these experiments, a strong dependence of the neutron yield on the laser radiation intensity was also found: when the maximum intensity was reduced by half, the neutron yield decreased by an order of magnitude, which can be explained by the fact that the formation of a channel in a dense plasma has a threshold [64].

The cross section for a fusion reaction initiated directly in the plasma substantially increases with increasing ion temperature of the plasma in nanostructured targets. Indeed, because the expansion velocity of ions is 10^7–10^8 cm s^{-1} already for intensities 10^{16} W cm^{-2}, the deuteron energy upon the explosion of nanostructures exceeds 1 keV [76]. This energy is directly transformed to the deuteron temperature. The velocity $\langle \sigma v \rangle_{dd}$ of the reactions ^{2}H(d, n)^{3}He, ^{2}H(d, p)^{4}He without a threshold rapidly grows with the deuteron energy, increasing from $\sim 10^{-35}$ cm^3 s^{-1} for the deuteron energy 50 eV to $\sim 10^{-19}$ cm^3 s^{-1} for the deuteron energy 5 keV. The experiments with such targets showed that for $Q \sim 0.002 - 0.06$ and $\tau \approx 35$ fs [10, 83, 135] the efficiency of neutron generation was not lower than that obtained at relativistic intensities (Table 4). Upon irradiation of a cluster deuterium jet, the neutron yield $N_n \lesssim 10^4$ neutron pulse^{-1} was obtained for $W \sim 0.1$ J, whereas in the case of a laser-modified deuterated titanium target, the neutron yield was $N_n \sim 5$ neutron pulse^{-1} for $W \sim 300$ μJ ($Q \sim 0.0025$ and $\tau \approx 200$ fs) [11].

The efficiency η_n of neutron generation obtained in different experiments is presented in Table 4. Here, two definitions of the efficiency are used: the energy efficiency $\eta_n = N_n/W$ and the efficiency $\eta_d = N_n/N_d$ over the number of accelerated deuterons N_d. Analysis of Table 4 shows that a fusion reaction proceeds most efficiently when high-contrast laser pulses with maximum intensity are used, i.e., when ions are accelerated upon 'punching' a dense plasma by a relativistic laser pulse [134].

A high neutron yield observed in paper [131] is probably explained by a large duration of laser pulses and optimal conditions for plasma heating and acceleration of a great number of deuterons in the region of interaction with cold

Table 4. Parameters of neutron sources.

Q	W/mJ	N_d/deuteron pulse^{-1}	ε_d/keV	σ_{dd}/mb	N_n/neutron pulse^{-1}	η_n/J^{-1}	η_d	τ_n/ps	References
1.5	20000	8×10^{13}	100	20	10^8	5000	0.9×10^{-6}	2 – 3	[131]
2.5	7000	10^{11}	550	70	10^7	1400	10^{-4}	< 1	[134]
0.3	200	4×10^{10}	200 – 300	35 – 45	140	0.7	3.5×10^{-9}	1 – 3	[132]
0.3	300	$\sim 10^{10}$	200 – 300	35 – 45	10^4	33.3	10^{-6}	< 1	[133]
0.05	200	10^{15}	2.5	0.2	10^4	100	10^{-10}	200	[83]
0.0025	0.3	10^8	2 – 3	0.2	5	15	5×10^{-8}	1	[11]

Notes: ε_d is the average deuteron energy; σ_{dd} is the average cross section for the DD reaction for energy ε_d; τ_n is the neutron-pulse duration.

deuterium ions at high density. An obvious drawback of the approach developed in paper [132] is a low density of cold deuterium ions around the plasma channel formed in the subcritical plasma. At present, the efficiency of a neutron source is lower at moderate intensities of laser radiation than at relativistic intensities, however, the cross section for the reaction is low for temperatures of the deuterium plasma achieved. The neutron yield in structured targets can be increased, in particular, by using more closely packed metal nanostructures of the brush type [86], which can be saturated by deuterium under pressure. In this case, we can expect the generation of up to 1000 neutron pulse^{-1} already for the laser pulse energy of 1 mJ.

A further increase in the number of fast deuterons induced by ultrashort pulses of relativistic intensity is related to the determination of the optimum (for the reaction proceeding) mechanism of ion acceleration, the laser radiation intensity and contrast. One should bear in mind that the cross section for the fusion DD reaction is a non-monotonic function of the energy of colliding ions, which has a broad maximum in the region 0.5 – 5 MeV. This means that an increase in the intensity above 10^{19} W cm^{-2}, when the mean energy of deuterons achieves 5 MeV, is inefficient. On the other hand, a number of fusion reactions in which neutrons are produced have the maximum cross sections in the energy region above 1 MeV [^{6}Li(d, n)^{7}Be, ^{12}C(d, n)^{13}N, ^{10}B(d, n)^{11}C, etc.], and the optimal intensity for such reactions can be substantially greater.

The important feature of a neutron thermonuclear USP plasma source is a short duration of a neutron pulse. The formation of the leading edge of a neutron pulse in nanostructured targets is determined by the thermalisation time of ions, i.e., by the time t_s of the structure spreading. The neutron-pulse duration is mainly limited by the gas-dynamic expansion of a plasma bunch into vacuum resulting in a rapid decrease in the mean density of the plasma and its cooling, and also by cooling of the ion component of the plasma due to electron – ion relaxation.

The neutron-pulse duration τ_n can be estimated from the expression $\tau_n \approx t_s + (\tau_a^{-1} + \tau_{ei}^{-1})^{-1}$, where τ_{ei} is the time of electron – ion relaxation. Because the neutron yield is proportional to a product of the square of the neutron density n_d by the plasma volume V [see (11)], we can assume that the time τ_a is the time for which the plasma density is halved. In the case of a cluster deuterium target, the electron – ion relaxation is absent, and the time $\tau_a \sim 100 - 300$ ps [135]. For a solid structured target, τ_{ei} and τ_a are of the same order of magnitude: $\tau_a \sim 1 - 10$ ps and $\tau_{ei} \sim 10$ ps [61] (one should also take into account that the rate of electron – ion relaxation decreases upon plasma expansion).

Therefore, the neutron-pulse duration is determined first of all by the plasma expansion into vacuum and is several picoseconds for a solid target and several hundreds of picoseconds for a cluster target. The time-of-flight neutron measurements performed in paper [135] confirm these estimates because, within the measurement error (1 ns), the scatter of the neutron energy corresponds to the expected energy of 2.45 MeV, i.e., the neutron-pulse duration is certainly shorter than 1 ns. The width ΔE_n of the energy spectrum of thermonuclear neutrons is determined by the scatter ΔE_d in the deuteron energy and the dependence of the neutron energy on the angle between the velocities of colliding deuterons [133]. Thus, the width of the spectrum of neutrons in experiments [133] was 700 keV, while for the cluster target, it was of about 200 keV [135]. This means that the duration τ_n will increase linearly with the distance from a source. For example, at a distance of 1m from the source, τ_n is ~ 0.15 μs for a cluster target and ~ 0.5 μs for a solid target. Note that, when moderate intensities are used, a neutron source proves to be quasi-monochromatic, with the spectral width of about 10 keV.

It is interesting to estimate the intensity I_n of a neutron source based on nanostructured targets:

$$I_n \approx \frac{N_n}{S\tau_n},$$

where $S = \pi r_0^2$, and $r_0 \sim 3 - 5$ μm. When 10^4 neutrons are generated, we have $I_n \sim 10^{22}$ neutron s^{-1} cm^{-2}, which exceeds the intensity of modern neutron generators.

Except fusion reactions producing neutrons, there exist a wide variety of fusion reactions producing gamma quanta [^{7}Li(p, γ)^{8}Be, the maximum of the reaction cross section is at 550 keV, ^{13}C(p, γ)^{14}N, 0.4 – 1 MeV], alpha particles [^{6}Li(p, α)^{3}He, 2 – 3 MeV, ^{6}Li(d, α)^{4}He, 0.7 – 4 MeV, ^{9}Be(p, α)^{3}Li, 0.6 – 1 MeV, ^{11}B(p, α)^{8}Be, 0.7 MeV], etc. Therefore, by initiating fusion reactions in the USP plasma, short pulses of other nuclear particles can be generated.

9. Conclusions

The analysis of the available experimental data has shown that the acceleration of electrons in the USP plasma up to the energies above 1 MeV at relativistic intensities ($Q > 1$) of laser pulses makes the USP plasma a source of corpuscular and electromagnetic radiation, which is capable of initiating nuclear processes in matter. The USP plasma is a source of fast highly charged ions for high-current ion accelerators [136] and of proton beams, which makes it possible to discuss new concepts of fast ignition of a fusion reaction [137].

A fundamentally new type of a nuclear radiation source based on a new generation of high-average power femtosecond technological lasers can be created already in the nearest years. The case in point is kilohertz tabletop laser systems, which provide, along with the intensity close to relativistic, an average output power up to 100 W. Such femtosecond technological lasers are already being developed at present [138]. In turn, the creation of laser-plasma sources of nuclear radiation involves first of all the optimisation of the parameters of the laser system and of the target for obtaining the maximum number of electrons with certain energy.

One of the most obvious and possibly commercially profitable applications may be the recovery of isotopes by irradiating targets with protons emitted from the USP plasma [68, 95]. Note also new possibilities for studying the radiation resistance of materials and chemonuclear reactions using ultrashort nuclear radiation pulses. Other promising applications concern the problems of medical physics and biophysics. These are tomography studies based on the use of proton and positron beams, radiative therapy, the study of the relative biological efficiency of radiation, etc.

Our analysis has also shown that a certain class of problems (excitation of low-lying nuclear levels and the laser control of gamma decay, the study of the population inversion at nuclear levels with energy from 10 to 100 keV, the

development of neutron thermonuclear sources) does not require, as a rule, relativistic intensities. Laser radiation with the parameter $Q \sim 0.01 - 0.1$ can be obtained using relatively inexpensive commercial tabletop femtosecond lasers of a moderate power ~ 1 W [139].

Acknowledgements. This work was supported by the Russian Foundation for Basic Research (Grants Nos 99-02-18343, 99-02-16093, 00-02-17302) and by the State Science and Technological Program 'Fundamental Metrology'.

References

1. Gordienko V M, Dzhidzhoev M S, Magnitskii S A, Platonenko V T *Moshchnye piko- i femtosekundnye lazernye sistemy; veshchestvo v sverkhsil'nykh svetovykh poilyakh* (High-Power Picosecond and Femtosecond Laser Systems. Matter in Superstrong Light Fields) (Advances in Science and Technology. Ser. Modern Problems of Laser Physics, Moscow: VINITI, 1991), vol. 4, p. 19; Biglov Z A, Gordienko V M *Moshchnye piko- i femtosekundnye lazernye sistemy; veshchestvo v sverkhsil'nykh svetovykh poilyakh* (High-Power Picosecond and Femtosecond Laser Systems. Matter in Superstrong Light Fields) (Advances in Science and Technology. Ser. Modern Problems of Laser Physics, Moscow: VINITI, 1991), vol. 4, p. 84
2. Backus S, Durfee C G, Murnane M M, Kapteyn H C *Rev. Sci. Instrum.* **69** 1207 (1998)
3. Perry M D, Pennington D, Stuart B C, et al. *Opt. Lett.* **24** 160 (1999)
4. Mukhin K N *Eksperimental'naya yadernaya fizika* (Experimental Nuclear Physics) (Moscow: Energoatomizdat, 1983), vol. 1
5. Luther-Davis B, Gamalii E G, et al. *Kvantovaya Elektron.* **19** 317 (1992) [*Quantum Electron.* **22** 289 (1992)]
6. Platonenko V T *Laser Physics* **2** 852 (1992)
7. Andreev A V, Gordienko V M, Dykhne A M, et al. *Pis'ma Zh. Eksp. Teor. Fiz.* **66** 312 (1997)
8. Andreev A V, Volkov R V, Gordienko V M, et al. *Zh. Eksp. Teor. Fiz.* **118** 1343 (2000)
9. Basov N G, Zakharov S D, Kryukov P G, et al. *Pis'ma Zh. Eksp. Teor. Fiz.* **8** 26 (1968)
10. Ditmire T, Zweiback J, Yanovsky V P, et al. *Nature* **398** 489 (1999)
11. Volkov R V, Golishnikov D M, Gordienko V M, et al. *Pis'ma Zh. Eksp. Teor. Fiz.* **72** 577 (2000)
12. Soom B, Chen H, Fisher Y, Meyerhofer D D *J. Appl. Phys.* **74** 5372 (1993)
13. Rousse A, Audebert P, Geindre J P, et al. *Phys. Rev. E* **50** 2200 (1994)
14. Varnavichus A, Vlasov T V, Volkov R V, et al. *Kvantovaya Elektron.* **30** 523 (2000) [*Quantum Electron.* **30** 523 (2000)
15. Gibbon P, Forster E *Plasma Phys. Control. Fusion* **38** 769 (1996)
16. Andreev A A, Mak A A, Yashin V E *Kvantovaya Elektron.* **24** 99 (1997) [*Quantum Electron.* **27** 95 (1997)
17. Andreev A A, Gamalii E G, Novikov V N, Tikhonchuk V T *Zh. Eksp. Teor. Fiz.* **101** 1808 (1992)
18. Gibbon P *Phys. Rev. Lett.* **73** 664 (1994)
19. Wharton K B, Hatchett S P, Wilks S C et al. *Phys. Rev. Lett.* **81** 822 (1998)
20. Zhang P, He J T, Chen D B, et al. *Phys. Rev. E* **57** R3746 (1998)
21. Gibbon P, Bell A R *Phys. Rev. Lett.* **68** 1535 (1992)
22. Meyerhofer D D, Chen H, Delletrez J A, et al. *Phys. Fluids B* **5** 2584 (1993)
23. Beg F N, Bell A R, Dangor A E et al. *Phys. Plasmas* **4** 447 (1997)
24. Kuhlke D, Herpers U, von der Linde D *Appl. Phys. Lett.* **50** 1785 (1987)
25. Volkov R V, Gordienko V M, Dzhidzhoev M S, et al. *Kvantovaya Elektron.* **25** 3 (1998) [*Quantum Electron.* **28** 1 (1998)]
26. Volkov R V, Gordienko V M, Mikheev P M, Savel'ev A B *Kvantovaya Elektron.* **30** 896 (2000) [*Quantum Electron.* **30** 896 (2000)]
27. Hatchett S P, Brown C G, Cowan T E et al. *Phys. Plasmas* **7** 2076 (2000)
28. Kruer W L, Estabrook K *Phys. Fluids* **28** 430 (1985)
29. Wilks S C, Kruer W L, Tabak M, Langdon A B *Phys Rev Lett.* **69** 1383 (1992)
30. Yu W, Yu M Y, Sheng Z M, Zhang J *Phys. Rev. E* **58** 2456 (1998)
31. Ruhl H, Sentoku Y, Mima K, et al. *Phys. Rev. Lett.* **82** 743 (1999)
32. Borisov A B, Borovskiy A V, Shirayev O B, et al. *Phys. Rev. A* **45** 5830 (1992)
33. Pukhov A, Meyer-ter-Vehn J *Phys. Plasmas* **5** 1880 (1998)
34. Borghesi M, MacKinnon A J, Bell A R, et al. *Phys. Rev. Lett.* **81** 112 (1998)
35. Tajima T, Dawson J M *Phys. Rev. Lett.* **43** 267 (1979)
36. Esarey E, Sprangle P, Ting A *IEEE Trans. Plasma Sci.* **24** 252 (1996)
37. Andreev N E, Gorbunov L M *Usp. Fiz. Nauk* **169** 53 (1999)
38. Sarkisov G S, Bychenkov V Yu, Novikov V N, et al. *Phys. Rev. E* **59** 7042 (1999)
39. Gahn C, Tsakiris G D, Meyer-ter-Vern J, et al. *Phys. Rev. Lett.* **83** 4772 (1999)
40. Amiranoff F, Baton S, Bernard D, et al. *Phys. Rev. Lett.* **81** 995 (1998)
41. Malka V, Faure J, Marques J R, et al. *Phys. Plasmas* **8** 2605 (2001)
42. Malka G, Fuchs J, Amiranoff F, et al. *Phys. Rev. Lett.* **79** 2053 (1997)
43. Guilietti D, Galimberti M, Gulietti A, Gizzi L A *Phys. Rev. E* **64** 5402R (2001)
44. Cowan T E, Hunt A W, Phillips T W, et al. *Phys. Rev. Lett.* **84** 903 (2000)
45. Pukhov A, Meyer-ter-Vern J *Phys. Rev. Lett.* **79** 2686 (1997)
46. Pukhov A, Sheng Z -M, Meyer-ter-Vern J *Phys. Plasmas* **6** 2847 (1999)
47. Pukhov A, Meyer-ter-Vehn J *Laser and Particle Beams* **17** 571 (1999)
48. Witte K, Gahn C, Meyer-ter-Vehn J, et al. *Plasma Phys. Control. Fusion* **41** B221 (1999)
49. Yu W, Bychenkov V, Sentoku Y, et al. *Phys. Rev. Lett.* **85** 570 (2000)
50. Wilks S C, Langdon A B, Cowan T E, et al. *Phys. Plasmas* **8** 542 (2001)
51. Tatarakis M, Lee P, Davies J R, et al. *Phys. Rev. Lett.* **81** 999 (1998)
52. Kmetec J D, Gordon C L, Macklin J J, et al. *Phys. Rev. Lett.* **68** 1527 (1992)
53. Perry M D, Sefcick J A, Cowan T, et al. *Rev. Sci. Instrum.* **70** 265 (1999)
54. McCall G H, Yuong F, Ehler A W, et al. *Phys. Rev. Lett.* **30** 1116 (1973)
55. Basov N G, Boiko V A, Zakharov S M, et al. *Pis'ma Zh. Eksp. Teor. Fiz.* **18** 314 (1973)
56. Andreev N E, Zakharenkov Yu A., Zorev N N, et al. *Zh. Eksp. Teor. Fiz.* **76** 976 (1979)
57. Gitomer S, Jones R D, Begay F, et al. *Phys. Fluids* **29** 2679 (1986)
58. Wickens L M, Allen J E, Rumsby P T *Phys. Rev. Lett.* **41** 243 (1978)
59. Young P E, Guethlein G, Wilks S C, et al. *Phys. Rev. Lett.* **76** 3128 (1996)

60. Andreev A A, Bayanov V I, Van'kov A B, et al. *Kvantovaya Elektron.* **23** 907 (1996) [*Quantum Electron.* **26** 884 (1996)]
61. Volkov R V, Golishnikov V M, Gordienko V M, et al. *Kvantovaya Elektron.* **31** 241 (2001) [*Quantum Electron.* **31** 241 (2001)]
62. Fews A P, Norreys P A, Beg F N, et al. *Phys. Rev. Lett.* **73** 1801 (1994)
63. Clark E L, Krushelnik K, Zepf M, et al. *Phys. Rev. Lett.* **85** 1654 (2000)
64. Esirkepov T Zh, Sentoku Y, Moma K, et al. *Pis'ma Zh. Eksp. Teor. Fiz.* **70** 80 (1999); Sentoku Y, Liseikina T V, Esirkepov T Zh, et al. *Phys. Rev. E* **62** 7271 (2000)
65. Maksimchuk A, Gu S, Flippo K, Umstadter D *Phys. Rev. Lett.* **84** 4108 (2000)
66. Snavely R A, Key M H, Hatchett S P *Phys. Rev. Lett.* **85** 2945 (2000)
67. Clark E L, Krushelnik K, Davies J R, et al. *Phys. Rev. Lett.* **84** 670 (2000)
68. Nemoto K, Maksimchuk A, Banerjee S, et al. *Appl. Phys. Lett.* **78** 595 (2001)
69. McPherson A, Thompson A, Borisov A B, et al. *Nature* **370** 631 (1994)
70. Ditmire T, Donnelly T, Falcone R, Perry M D *Phys. Rev. Lett.* **75** 3122 (1995)
71. Murnane M M, Kapteyn H C, Gordon S P, et al. *Appl. Phys. Lett.* **62** 1068 (1993)
72. Gordon S P, Donnelly T, Sullivan A, et al. *Opt. Lett.* **19** 484 (1994)
73. Volkov R V, Gordienko V M, Dzhidzhoev M S, et al. *Kvantovaya Elektron.* **24** 1114 (1997) [*Quantum Electron.* **27** 1081 (1997)]
74. Nishikawa T, Nakano H, Ahn H, Uesugi N *Appl. Phys. Lett.* **70** 1653 (1997)
75. Wulker C, Theobald W, Gnass D R *Appl. Phys. Lett.* **68** 1338 (1996)
76. Ditmire T, Springate E, Tisch J W G, et al. *Phys. Rev. A* **57** 369 (1998)
77. Schroeder W A, Omenetto F G, Borisov A B, et al. *J. Phys. B* **31** 5031 (1998)
78. Krainov V P, Smirnov M B *Usp. Fiz. Nauk* **170** 969 (2000)
79. Springate E, Hay N, Tisch J W G, et al. *Phys. Rev. A* **61** 63201 (2000)
80. Lezius M, Dobosz S, Normand D, Schmidt M *Phys. Rev. Lett.* **80** 261 (1998)
81. Ishikawa K, Blenski T *Phys. Rev. A* **62** 63204 (2000)
82. Springate E, Hay N, Tissch J W G, et al. *Phys. Rev. A* **61** 44101 (2000)
83. Zweiback J, Smith R A, Cowan T E, et al. *Phys. Rev. Lett.* **84** 2634 (2000)
84. Gordienko V M, Savel'ev A B *Usp. Fiz. Nauk* **169** 78 (1999)
85. Nishikawa T, Nakano H, Uesugi N, Serikawa T *Appl. Phys. B* **66** 567 (1998)
86. Gordienko V M, Dzhidzhoev M S, Joukov M A, et al. In: *Superstrong Fields in Plasmas. AIP Conference Proceedings* (New York, 1998), vol. 426, p. 241
87. Kulsar G, AlMawlawi D, Budnik F W, et al. *Phys. Rev. Lett.* **84** 5149 (2000)
88. Boyer K, Luk T S, Rhodes C K *Phys. Rev. Lett.* **60** 557 (1988)
89. Askar'yan G A *Pis'ma Zh. Eksp. Teor. Fiz.* **48** 179 (1988)
90. Shkolnikov P L, Kaplan A E, Pukhov A, Meyer-ter-Vehn J *Appl. Phys. Lett.* **24** 3471 (1997)
91. Bychenkov V Yu, Tikhonchuk V T, Tolokonnikov V T *Zh. Eksp. Teor. Fiz.* **115** 2080 (1999)
92. Perry M D, Cowan T, Pennington D, et al. *Abstracts of IQEC'98 OSA Technical Digest Series* (Washington, OSA, 1998), vol. 7, p. 74.
93. Perry M D, Sefcick J A, Cowan T, et al. *Rev. Sci. Instrum.* **70** 265 (1999)
94. Norreys P A, Santala M, Clark E, et al. *Phys. Plasmas* **6** 2150 (1999)
95. Ledingham K W D, Norreys P A *Contemporary Physics* **40** 367 (1999)
96. Ledingham K W D, Spencer I, McCanny T, et al. *Phys. Rev. Lett.* **84** 899 (2000)
97. Schwoerer H, Gibbon P, Dusterer S, et al. *Phys. Rev. Lett.* **86** 2317 (2001)
98. Shkolnikov P L, Kaplan A E *J. Nonlinear Opt. Phys. Mater.* **6** 161 (1997)
99. Gryaznykh D A, Kandiev Ya Z, Lykov V A *Pis'ma Zh. Eksp. Teor. Fiz.* **67** 239 (1998)
100. Cowan T E, Perry M D, Key M H, et al. *Laser Part. Beams* **17** 773 (1999)
101. Gahn C, Tsakiris G D, Pretzler G, et al. *Appl. Phys. Lett.* **77** 2662 (2000)
102. Santala M I K, Zepf M, Beg F N, et al. *Appl. Phys. Lett.* **78** 19 (2001)
103. Yamagiwa M, Koga J *J. Phys. D* **32** 2526 (1999)
104. Morita M *Prog. Theor. Phys.* **49** 1574 (1973)
105. Andreev A V, Gordienko V M, Savel'ev A B *Laser Physics* **10** 537 (2000)
106. Elton R C *X-ray Lasers* (Boston: Academic Press, 1990)
107. Andreev A V *Vestn. Mosk. Univ. Ser. R: Fiz. Astron.* **35** (3) 28 (1994)
108. Collins C B, Davanloo F, et al. *Phys. Rev. C* **61** 4305 (2000)
109. Groshev L V, Shapiro I S *Spektroskopiya atomnykh yader* (Spectroscopy of Atomic Nuclei) (Moscow,1952)
110. Attallah F, Aiche M, Chemin G F, et al. *Phys. Rev. Lett.* **75** 1715 (1995)
111. Chumakov A I, Baron A Q R, Arthur J, et al. *Phys. Rev. Lett.* **75** 549 (1995)
112. Seto M, Yoda Y, Kikuta S, et al. *Phys. Rev. Lett.* **74** 3828 (1995)
113. Letokhov V S *Kvantovaya Elektron.* (4) 125 (1973) [*Sov. J. Quantum Electron.* **3** 360 (1973)]
114. Tkalya E V *Zh. Eksp. Teor. Fiz.* **102** 379 (1992)
115. Izawa Y, Yamanaka C *Phys. Lett. B* **88** 59 (1979)
116. Arutyunyan R V, Bol'shov L A, Vikharev V D, et al. *Yad. Fiz.* **53** 36 (1991)
117. Tkalya E V *Pis'ma Zh. Eksp. Teor. Fiz.* **53** 441 (1991)
118. Andreev A V, Gordienko V M, Savel'ev A B *Preprint of Department of Physics, Moscow State University, no 1* (Moscow, 1997)
119. Andreev A V, Volkov R V, Gordienko V M, et al. *Pis'ma Zh. Eksp. Teor. Fiz.* **69** 343 (1999)
120. Andreev A V, Volkov R V, Gordienko V M, et al. *Kvantovaya Elektron.* **26** 55 (1999) [*Quantum Electron.* **29** 55 (1999)]
121. Kishimoto S, Yoda Y, Seto M, et al. *Phys. Rev. Lett.* **85** 1831 (2000)
122. Arutyunyan R V, Bol'shov L A, Soldatov A A, et al. *Yad. Fiz.* **48** 1301 (1988)
123. Gol'danskii V I, Namiot V A *Pis'ma Zh. Eksp. Teor. Fiz.* **23** 495 (1976)
124. Letokhov V S, Yukov E A *Laser Physics* **4** 382 (1994)
125. Andreev A V, Gordienko V M, Savel'ev A B *ICONO'2001* (Minsk, Belarus, 2001), p. 4
126. Attallah F, Aiche M, Chemin G F, et al. *Phys. Rev. C* **55** 1665 (1997)
127. Strizhev V F, Tkalya E V *Zh. Eksp. Teor. Fiz.* **99** 697 (1991)
128. Carreyre T, Harston M R, Aiche M, et al. *Phys. Rev. C* **62** 24311 (2000)
129. Andreev A V, Gordienko V M, Savel'ev A B, et al. *Kvantovaya Elektron.* **31** 567 (2001) [*Quantum Electron.* **31** 567 (1999)]
130. Bruckner K, Jorna C *Upravlyaemyi termoyadernyi sintez* (Controlled Thermonuclear Fusion) (Moscow: Атомиздат, 1977)?
131. Norreys P A, Fews A P, Beg F N, et al. *Plasma Phys. Control. Fusion* **40** 175 (1998)

132. Pretzler G, Saemann A, Pukhov A, et al. *Phys. Rev. E* **58** 1165 (1998)
133. Hilsher D, Berndt O, Enke M, et al. *Phys. Rev. E* **64** 16414 (2001)
134. Disdier L, Garconnet J -P, Malka G, Miquel J -L *Phys. Rev. Lett.* **82** 1454 (1999)
135. Zweiback J, Cowan T.E, Smith R A, et al. *Phys. Rev. Lett.* **85** 3640 (2000)
136. Irons F, Pikock H, Pis R *Kvantovaya Elektron.* (7) 20 (1972) [*Sov. J. Quantum Electron.* **2** 13 (1972)]
137. Roth M, Cowan T E, Key MH, et al. *Phys. Rev. Lett.* **86** 436 (2001)
138. Backus S, Bartels R, Thompson S, et al. *Opt. Lett.* **26** 465 (2001)
139. Gordienko V M *Preprint of Department of Physics, Moscow State University, no. 13/2000* (Moscow, 2000)